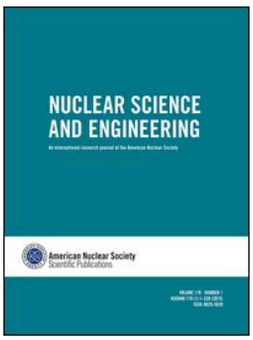

Nuclear Science and Engineering

ISSN: 0029-5639 (Print) 1943-748X (Online) Journal homepage: http://www.tandfonline.com/loi/unse20

The Relationship between the Coarse-Mesh Finite Difference and the Coarse-Mesh Diffusion Synthetic Acceleration Methods

Edward W. Larsen & Blake W. Kelley

To cite this article: Edward W. Larsen & Blake W. Kelley (2014) The Relationship between the Coarse-Mesh Finite Difference and the Coarse-Mesh Diffusion Synthetic Acceleration Methods, Nuclear Science and Engineering, 178:1, 1-15

To link to this article: http://dx.doi.org/10.13182/NSE13-47

NUCLEAR SCIENCE AND ENGINEERING: **178**, 1–15 (2014)

The Relationship Between the Coarse-Mesh Finite Difference and the Coarse-Mesh Diffusion Synthetic Acceleration Methods

Edward W. Larsen* and Blake W. Kelley

University of Michigan, Department of Nuclear Engineering and Radiological Sciences
Ann Arbor, Michigan 48109-2104

Received June 10, 2013
Accepted January 4, 2014
http://dx.doi.org/10.13182/NSE13-47

Abstract—*The coarse-mesh finite difference (CMFD) and the coarse-mesh diffusion synthetic acceleration (CMDSA) methods are widely used, independently developed methods for accelerating the iterative convergence of deterministic neutron transport calculations. In this paper, we show that these methods have the following theoretical relationship: If the standard notion of diffusion synthetic acceleration as a fine-mesh method is straightforwardly generalized to a coarse-mesh method, then the linearized form of the CMFD method is algebraically equivalent to a CMDSA method. We also show theoretically (via Fourier analysis) and experimentally (via simulations) that for fixed-source problems, the CMDSA and CMFD methods have nearly identical convergence rates. Our numerical results confirm the close theoretically predicted relationship between these methods.*

I. INTRODUCTION

For many years, large-scale deterministic neutron transport codes have used source iteration with an acceleration scheme to iteratively converge the scattering and fission sources.[1] The source iteration method alone converges rapidly only for problems having high absorption or high leakage probabilities; when the absorption and leakage probabilities are both small (and neutron histories are long), the source iteration scheme converges extremely slowly. Early acceleration methods included fine- and coarse-mesh rebalancing; these were superseded by various forms of diffusion synthetic acceleration[1–5] (DSA). Later, the coarse-mesh finite difference (CMFD) method was developed independently.[6–9]

Outwardly, the DSA and CMFD methods have certain similarities: Both methods define a single iteration to consist of a high-order transport sweep, followed by a low-order diffusion calculation. However, the two methods have significant differences. First, DSA is linear, and CMFD is nonlinear. Second, DSA is traditionally used as a fine-grid method in which the spatial grids for the transport and diffusion calculations are the same, whereas CMFD is normally used as a coarse-grid method in which the spatial grid for the diffusion equation is coarser than the spatial grid for the transport equation. Third, in DSA, the low-order solution is a fine-grid linear correction to the high-order scalar flux, whereas in CMFD, the low-order solution is a coarse-grid volume-averaged scalar flux.

In 2003, Cho and Park Fourier-analyzed a linearized CMFD (LCMFD) method.[8] They showed, theoretically and experimentally, that the CMFD method converges rapidly when the coarse cells are less than 1 mean free path (mfp) thick, but as the coarse cells become thicker, the method degrades in performance and ultimately diverges. Cho and Park observed that this behavior is qualitatively similar to the convergence properties of an inconsistent DSA method, in which (a) the transport and diffusion grids are the same and (b) a standard discretization of the diffusion equation is used, which is not consistent with the transport discretization.[1,4]

DSA is commonly understood to be a fine-mesh method, in which the spatial grids for the high-order transport and the low-order diffusion equations are the same, but it is straightforward to allow the low-order diffusion problem to be discretized on a coarser spatial grid.

*E-mail: edlarsen@umich.edu

The resulting coarse-mesh DSA (CMDSA) method is usually inconsistent—the diffusion discretization is not related to the transport discretization in a way that ensures rapid convergence for all fine- or coarse-mesh thicknesses. To repeat, if the consistency issue is put aside, there is no conceptual difficulty implementing the DSA method using a coarser spatial mesh for the low-order diffusion calculation than for the higher-order transport equation.

In this paper, we apply the above ideas to show that the CMDSA and CMFD methods have the following theoretical relationship:

1. The linearized form of the CMFD method is algebraically equivalent to a CMDSA method.

2. A Fourier analysis accurately predicts the convergence properties of the CMDSA method. (This extends the previous work by Cho and Park.[8])

3. In numerical simulations of fixed-source problems, the (linear) CMDSA and (nonlinear) CMFD methods have nearly the same convergence properties. Hence, the Fourier analysis results accurately describe both the linear CMDSA (= LCMFD) and the nonlinear CMFD methods.

Therefore, rather than being two unrelated methods, DSA and CMFD have close theoretical links. Of course, there are significant differences—the main one being that the low-order DSA and CMDSA problems are linear, while the low-order CMFD problem is nonlinear. (Because of its nonlinearity, CMFD is easier to apply to the outer iterations of eigenvalue problems—an advantage of CMFD. However, the linear CMDSA method will not become unstable if a scalar flux iterate becomes zero or negative—an advantage of CMDSA.) Nonetheless, for problems in which both methods can be used, the Fourier analysis predicts and our numerical results confirm that the two methods have nearly the same convergence properties.

This paper is a revised version of a recent conference paper.[10] The remainder of the paper is organized as follows. In Sec. II, a one-dimensional S_N fixed-source problem is described, for which the (linear) CMDSA and (nonlinear) CMFD methods are formulated. In Sec. III the CMFD method is linearized, and the resulting LCMFD method is shown to be algebraically equivalent to a CMDSA method. In Sec. IV the Fourier analysis for the CMDSA method is developed for the step characteristic spatial discretization method with p fine spatial cells per coarse cell; the Fourier analysis is used to predict the spectral radius of this method. (This section reviews the previous work of Cho and Park.[8]) Section V presents the results of numerical experiments, confirming the theoretical predictions from Sec. III and showing that the (linear) CMDSA and (nonlinear) CMFD methods have nearly the same convergence properties. Section VI concludes the paper with a brief discussion.

II. THE CMFD AND CMDSA METHODS

Here, we describe the CMFD and CMDSA methods for a planar geometry fixed-source problem on the system $0 \le x \le X$:

$$\mu \frac{\partial \psi}{\partial x}(x,\mu) + \sigma_t(x)\psi(x,\mu) = \frac{\sigma_s(x)}{2}\int_{-1}^{1} \psi(x,\mu')d\mu' + \frac{q(x)}{2} , \tag{1a}$$

$$\psi(0,\mu) = \psi^b(\mu), \ 0 < \mu \le 1 , \tag{1b}$$

and

$$\psi(X,\mu) = \psi^b(\mu), \ -1 \le \mu < 0 . \tag{1c}$$

The notation here is standard.

Using the familiar discrete ordinates approximation in angle and an arbitrary weighted diamond approximation in space, we discretize Eqs. (1) as follows:

$$\frac{\mu_n}{h_j}\left(\psi_{n,j+1/2} - \psi_{n,j+1/2}\right) + \sigma_{t,j}\psi_{n,j} = \frac{\sigma_{s,j}}{2}\sum_{m=1}^{N}\psi_{m,j}w_m + \frac{q_j}{2} , \tag{2a}$$

$$\psi_{n,j} = \left(\frac{1+\alpha_{n,j}}{2}\right)\psi_{n,j+1/2} + \left(\frac{1-\alpha_{n,j}}{2}\right)\psi_{n,j-1/2} , \tag{2b}$$

$$\psi_{n,1/2} = \psi_n^b, \ \mu_n > 0 , \tag{2c}$$

$$\psi_{n,J+1/2} = \psi_n^b, \ \mu_n < 0 . \tag{2d}$$

The notation in Eqs. (2) is also standard. The subscript j, running over $1 \le j \le J$, denotes the (fine) spatial cell, which has width h_j, cross sections $\sigma_{t,j}$ and $\sigma_{s,j}$, and constant internal source q_j. The subscript n, running from $1 \le n \le N$, denotes the direction cosine of flight. The constants $\alpha_{n,j}$ determine the specific spatial discretization method, e.g.,

$$\alpha_{n,j} = \begin{cases} 0 & , \text{ Diamond Difference} , \\ \dfrac{1+e^{-\sigma_{t,j}h_j/\mu_n}}{1-e^{-\sigma_{t,j}h_j/\mu_n}} - \dfrac{2\mu_n}{\sigma_{t,j}h_j} & , \text{ Step Characteristic} . \end{cases} \tag{3}$$

The CMFD and CMDSA methods begin each iteration with a standard fine-mesh transport sweep. At the beginning of the ℓ'th iteration, the fine-mesh cell-averaged scalar fluxes,

$$\phi_{0,j}^{(\ell)} = \sum_{n=1}^{N} \psi_{n,j}^{(\ell)} w_n, \quad 1 \le j \le J \ , \tag{4}$$

are assumed to be known, either from the previous iteration or from the initial guess if $\ell = 0$. Then, the following version of Eqs. (2):

$$\frac{\mu_n}{h_j}\left(\psi_{n,j+1/2}^{(\ell+1/2)} - \psi_{n,j-1/2}^{(\ell+1/2)}\right) + \sigma_{t,j}\psi_{n,j}^{(\ell+1/2)} = \frac{\sigma_{s,j}}{2}\phi_{0,j}^{(\ell)} + \frac{q_j}{2} \ , \tag{5a}$$

$$\psi_{n,j}^{(\ell+1/2)} = \left(\frac{1+\alpha_{n,j}}{2}\right)\psi_{n,j+1/2}^{(\ell+1/2)} + \left(\frac{1-\alpha_{n,j}}{2}\right)\psi_{n,j-1/2}^{(\ell+1/2)} \ , \tag{5b}$$

$$\psi_{n,1/2}^{(\ell+1/2)} = \psi_n^b, \quad \mu_n > 0 \ , \tag{5c}$$

$$\psi_{n,J+1/2}^{(\ell+1/2)} = \psi_n^b, \quad \mu_n < 0 \ , \tag{5d}$$

is solved by a standard transport sweep for the $\psi^{(\ell+1/2)}$ unknowns. During this sweep, the cell-averaged fluxes and (for CMFD) the cell-edge currents are computed and stored:

$$\phi_{0,j}^{(\ell+1/2)} = \sum_{n=1}^{N} \psi_{n,j}^{(\ell+1/2)} w_n \ , \tag{6a}$$

$$\phi_{1,j+1/2}^{(\ell+1/2)} = \sum_{n=1}^{N} \mu_n \psi_{n,j+1/2}^{(\ell+1/2)} w_n \ . \tag{6b}$$

In the classic source iteration method, the fine-mesh scalar fluxes for iteration $\ell+1$ are defined simply from Eqs. (6) by

$$\phi_{0,j}^{(\ell+1)} = \phi_{0,j}^{(\ell+1/2)}, \quad 1 \le j \le J \ . \tag{7}$$

However, this method converges slowly for problems in which the system is optically thick and highly scattering. The CMDSA and CMFD methods retain Eqs. (5) and (6) but not Eq. (7); this definition of $\phi_{0,j}^{(\ell+1)}$ is replaced by a more sophisticated calculation, which can significantly reduce the total number of iterations.

To proceed, we introduce the notation for the coarse spatial grid. This grid contains $K \le J$ disjoint coarse spatial cells, each consisting of a contiguous union of fine-mesh cells. If p_k is the number of fine cells in coarse cell k (ordered from left to right as k increases), then for $0 \le k \le K$,

$$P_0 = 0 \ , \tag{8a}$$

$$P_k = \sum_{k'=1}^{k} p_{k'} = \text{number of fine cells in the first } k \text{ coarse cells} \ , \tag{8b}$$

$$P_K = J = \text{total number of fine cells} \ , \tag{8c}$$

and

$$X_{k+1/2} = x_{P_k+1/2} = \text{right edge of the } k' \text{th coarse cell} = \text{left edge of the } (k+1)' \text{th coarse cell.} \tag{9}$$

The fine and coarse spatial cells are depicted in Fig. 1.

To proceed, we introduce the notation

$$\sum_{j \in k} = \sum_{j=P_k+1}^{P_{k+1}} = \text{sum of all fine cells } j \text{ in coarse cell } k, \tag{10}$$

and we define the coarse cell quantities:

$$\Delta_k = \sum_{j \in k} h_j = \text{width of coarse cell } k, \tag{11a}$$

$$\Phi_{0,k} = \frac{1}{\Delta_k}\sum_{j \in k} \phi_{0,j} h_j = \text{volume-averaged scalar flux in coarse cell } k, \tag{11b}$$

$$Q_k = \frac{1}{\Delta_k}\sum_{j \in k} q_j h_j = \text{volume-averaged source in coarse cell } k \ , \tag{11c}$$

$$\Phi_{1,k+1/2} = \phi_{1,P_k+1/2} = \text{current on the right edge of coarse cell } k \ , \tag{11d}$$

$$\Sigma_{u,k} = \frac{1}{\Delta_k}\sum_{j \in k} \sigma_{u,j} h_j = \text{volume-averaged cross section in coarse cell } k \ \ (u = t,s,\gamma) \ , \tag{11e}$$

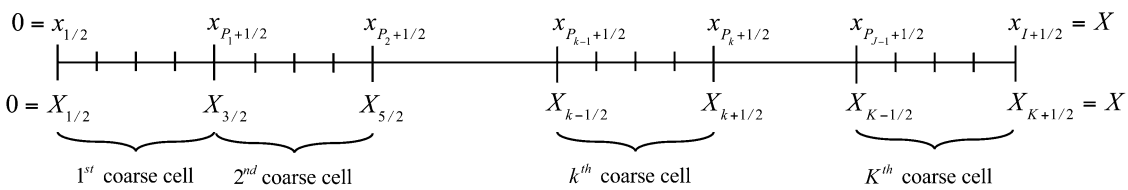

Fig. 1. Fine and coarse spatial grids.

$$\Sigma_{u,k}^{(\ell+1/2)} = \frac{\sum_{j\in k}\sigma_{u,j}\phi_{0,j}^{(\ell+1/2)}h_j}{\sum_{j\in k}\phi_{0,j}^{(\ell+1/2)}h_j} = \text{flux-weighted cross section in coarse cell } k \ (u=t,s,\gamma) \ . \tag{11f}$$

(Fine-cell quantities are denoted by lower-case letters; coarse-cell quantities are denoted by upper-case letters.)

II.A. Coarse-Mesh Finite Difference

To derive the CMFD method, we operate on Eq. (5a) by $\sum_{n=1}^{N}(\cdot)w_n$ to get

$$\frac{1}{h_j}\left(\phi_{1,j+1/2}^{(\ell+1/2)}-\phi_{1,j-1/2}^{(\ell+1/2)}\right)+\sigma_{t,j}\phi_{0,j}^{(\ell+1/2)}=\sigma_{s,j}\phi_{0,j}^{(\ell)}+q_j \ . \tag{12}$$

Then, we operate on Eq. (12) by $\sum_{j\in k}(\cdot)h_j$. Using the definitions (11), we obtain

$$\Phi_{1,k+1/2}^{(\ell+1/2)}-\Phi_{1,k-1/2}^{(\ell+1/2)}+\Sigma_{t,k}^{(\ell+1/2)}\Phi_{0,k}^{(\ell+1/2)}\Delta_k = \Sigma_{s,k}^{(\ell)}\Phi_{0,k}^{(\ell)}\Delta_k+Q_k\Delta_k \ . \tag{13}$$

Next, we define $\hat{D}_{k+1/2}^{(\ell+1/2)}$ at each interior coarse cell edge $(1\le k\le K-1)$ by

$$\Phi_{1,k+1/2}^{(\ell+1/2)} = -\frac{2}{3}\left(\frac{\Phi_{0,k+1}^{(\ell+1/2)}-\Phi_{0,k}^{(\ell+1/2)}}{\Sigma_{t,k+1}^{(\ell+1/2)}\Delta_{k+1}+\Sigma_{t,k}^{(\ell+1/2)}\Delta_k}\right) +\hat{D}_{k+1/2}^{(\ell+1/2)}\left(\Phi_{0,k+1}^{(\ell+1/2)}+\Phi_{0,k}^{(\ell+1/2)}\right) \ . \tag{14}$$

(We note that $\hat{D}_{k+1/2}^{(\ell+1/2)}$ can be calculated at the conclusion of each transport sweep and that this quantity is a *transport correction to Fick's Law*, which vanishes if Fick's Law exactly relates the current to the discretized derivative of the scalar flux.) At the left edge of the system, we define $B_{1/2}^{(\ell+1/2)}$ by

$$\begin{aligned}2\Phi_{1,1/2}^{+} &= 2\sum_{\mu_n>0}\mu_n\psi_n^b w_n \\ &= \sum_{n=1}^{N}(\mu_n+|\mu_n|)\psi_{n,1/2}^{(\ell+1/2)}w_n \\ &= \Phi_{1,1/2}^{(\ell+1/2)}+\left(\frac{\sum_{n=1}^{N}|\mu_n|\psi_{n,1/2}^{(\ell+1/2)}w_n}{\sum_{n=1}^{N}\Psi_{n,1}^{(\ell+1/2)}w_n}\right)\Phi_{0,1}^{(\ell+1/2)} \\ &= \Phi_{1,1/2}^{(\ell+1/2)}+\left(B_{1/2}^{(\ell+1/2)}\right)\Phi_{0,1}^{(\ell+1/2)} \ ,\end{aligned} \tag{15a}$$

and at the right edge of the system, we define $B_{K+1/2}^{(\ell+1/2)}$ by

$$\begin{aligned}2\Phi_{1,K+1/2}^{+} &= 2\sum_{\mu_n<0}|\mu_n|\psi_n^b w_n \\ &= \sum_{n=1}^{N}(-\mu_n+|\mu_n|)\psi_{n,J+1/2}^{(\ell+1/2)}w_n = -\Phi_{1,K+1/2}^{(\ell+1/2)} \\ &\quad+\left(\frac{\sum_{n=1}^{N}|\mu_n|\psi_{n,J+1/2}^{(\ell+1/2)}w_n}{\sum_{n=1}^{N}\Psi_{n,K}^{(\ell+1/2)}w_n}\right)\Phi_{0,K}^{(\ell+1/2)} \\ &= -\Phi_{1,K+1/2}^{(\ell+1/2)}+\left(B_{K+1/2}^{(\ell+1/2)}\right)\Phi_{0,K}^{(\ell+1/2)} \ .\end{aligned} \tag{15b}$$

At the conclusion of the transport sweep: (a) the $\psi^{(\ell+1/2)}$ quantities have been determined, (b) Eqs. (13) are satisfied for each coarse cell k, (c) Eq. (14) defines $\hat{D}_{k+1/2}^{(\ell+1/2)}$ at interior coarse cell edges, and (d) Eqs. (15) define $B_{1/2}^{(\ell+1/2)}$ and $B_{K+1/2}^{(\ell+1/2)}$ at the left and right edges of the system. It is now possible to define, in terms of these equations, *acceleration* equations for the coarse cell-averaged scalar fluxes and the coarse cell-edge currents.

In the CMFD method, $\Phi_{0,k}^{(\ell+1)}$ and $\Phi_{1,k+1/2}^{(\ell+1)}$ are defined to be the solutions of the following altered versions of Eqs. (13), (14) and (15):

$$\Phi_{1,k+1/2}^{(\ell+1)}-\Phi_{1,k-1/2}^{(\ell+1)}+\Sigma_{a,k}^{(\ell+1/2)}\Phi_{0,k}^{(\ell+1)}\Delta_k = Q_k\Delta_k \ , \tag{16a}$$

$$\Phi_{1,k+1/2}^{(\ell+1)} = -\frac{2}{3}\left(\frac{\Phi_{0,k+1}^{(\ell+1)}-\Phi_{0,k}^{(\ell+1)}}{\Sigma_{t,k+1}^{(\ell+1/2)}\Delta_{k+1}+\Sigma_{t,k}^{(\ell+1/2)}\Delta_k}\right) +\hat{D}_{k+1/2}^{(\ell+1/2)}\left(\Phi_{0,k+1}^{(\ell+1)}+\Phi_{0,k}^{(\ell+1)}\right) \ , \tag{16b}$$

$$2\Phi_{1,1/2}^{+} = \Phi_{1,1/2}^{(\ell+1)}+(B_{1/2}^{(\ell+1/2)})\Phi_{0,1}^{(\ell+1)} \ , \tag{16c}$$

$$2\Phi_{1,K+1/2}^{+} = -\Phi_{1,K+1/2}^{(\ell+1)}+(B_{K+1/2}^{(\ell+1/2)})\Phi_{0,J}^{(\ell+1)} \ . \tag{16d}$$

The coarse cell-edge currents in these equations, $\Phi_{1,k+1/2}^{(\ell+1)}$, can be algebraically eliminated, yielding a tridiagonal system of K equations for the coarse cell-averaged scalar fluxes $\Phi_{0,k}^{(\ell+1)}$, $1\le k\le K$. After these quantities are obtained, the accelerated fine-cell scalar fluxes are defined as

$$\phi_{0,j}^{(\ell+1)} = \phi_{0,j}^{(\ell+1/2)}\left(\frac{\Phi_{0,k}^{(\ell+1)}}{\Phi_{0,k}^{(\ell+1/2)}}\right), \quad j\in k, \quad 1\le k\le K \ . \tag{17}$$

This completes the description of the CMFD method. The logic underlying this method is that if the transport corrections to diffusion $\hat{D}_{k+1/2}^{(\ell+1/2)}$ are small, then these quantities can be lagged in Eq. (16b), and the resulting iterative method will converge rapidly. For problems in which the coarse cells are not optically thick, this logic is valid, as we show below.

II.B. Coarse-Mesh Diffusion Synthetic Acceleration

To derive the CMDSA method, we define the exact fine-mesh iteration errors after the ℓ'th transport sweep:

$$f_{1,j+1/2} = \phi_{1,j+1/2} - \phi_{1,j+1/2}^{(\ell+1/2)} , \tag{18a}$$

$$f_{0,j} = \phi_{0,j} - \phi_{0,j}^{(\ell+1/2)} . \tag{18b}$$

These can easily be shown, using Eq. (5a), to satisfy

$$\frac{1}{h_j}(f_{1,j+1/2} - f_{1,j-1/2}) + \sigma_{a,j} f_{0,j} = \sigma_{s,j}\left(\phi_{0,j}^{(\ell+1/2)} - \phi_{0,j}^{(\ell)}\right), \quad 1 \le k \le K .$$

Equivalently,

$$\frac{1}{h_j}(f_{1,j+1/2} - f_{1,j-1/2}) + \Sigma_{a,k} f_{0,j} = \sigma_{s,j}\left(\phi_{0,j}^{(\ell+1/2)} - \phi_{0,j}^{(\ell)}\right) + (\Sigma_{a,k} - \sigma_{a,j}) f_{0,j} . \tag{19}$$

Operating on this result by $\sum_{j\in k}(\cdot)h_j$ and defining the coarse cell quantities

$$F_{0,k} = \frac{1}{\Delta_k}\sum_{j\in k} f_{0,j} h_j , \tag{20a}$$

$$F_{1,k+1/2} = f_{1,P_k+1/2} , \tag{20b}$$

we get

$$F_{1,k+1/2} - F_{1,k-1/2} + \Sigma_{a,k} F_{0,k} \Delta_k = \sum_{j\in k} \sigma_{s,j}\left(\phi_{0,j}^{(\ell+1/2)} - \phi_{0,j}^{(\ell)}\right) h_j + \sum_{j\in k} (\Sigma_{a,k} - \sigma_{a,j}) f_{0,j} h_j . \tag{21}$$

Equations (21) are J equations for the $2J+1$ quantities $F_{0,k}$ and $F_{1,k+1/2}$. (Also, the fine-mesh quantities $f_{0,j}$ on the right side of these equations are not known.)

In the CMDSA method, $F_{0,k}^{(\ell+1)}$ and $F_{1,k+1/2}^{(\ell+1)}$ are determined by the following version of Eq. (21):

$$F_{1,k+1/2}^{(\ell+1)} - F_{1,k-1/2}^{(\ell+1)} + \Sigma_{a,k} F_{0,k}^{(\ell+1)} \Delta_k = \sum_{j\in k} \sigma_{s,j}\left(\phi_{0,j}^{(\ell+1/2)} - \phi_{0,j}^{(\ell)}\right) h_j , \quad 1 \le k \le K , \tag{22a}$$

together with the diffusion approximation:

$$F_{1,k+1/2}^{(\ell+1)} = -\frac{2}{3}\left(\frac{F_{0,k+1}^{(\ell+1)} + F_{0,k}^{(\ell+1)}}{\Sigma_{t,k+1}\Delta_{k+1} + \Sigma_{t,k}\Delta_k}\right), \quad 1 \le k \le K-1 , \tag{22b}$$

$$0 = F_{1,1/2}^{(\ell+1)} + \beta F_{0,1}^{(\ell+1)} , \tag{22c}$$

$$0 = -F_{1,K+1/2}^{(\ell+1)} + \beta F_{0,K}^{(\ell+1)} , \tag{22d}$$

where

$$\beta \equiv \frac{1}{2}\left(\sum_{n=1}^{N} |\mu_n| w_n\right) \approx \frac{1}{2} . \tag{23}$$

The cell-edge current corrections $F_{1,k+1/2}^{(\ell+1)}$ in Eqs. (22) can be algebraically eliminated, yielding a tridiagonal system of K equations for $F_{0,k}^{(\ell+1)}$, $1 \le k \le K$. After these quantities are calculated, the accelerated fine-cell scalar fluxes are defined as

$$\phi_{0,j}^{(\ell+1)} = \phi_{0,j}^{(\ell+1/2)} + F_{0,k}^{(\ell+1)} , \quad j \in k , \quad 1 \le k \le K . \tag{24}$$

This completes the description of the CMDSA method. The logic underlying this method is that if (a) the second term on the right side of Eq. (21) is sufficiently small that it can be neglected and (b) the discrete Fick's Law in Eq. (22b) is sufficiently accurate, then the solution of Eqs. (22) should yield a sufficiently accurate coarse-grid correction to the fine-grid scalar fluxes that the resulting iteration scheme will converge rapidly. For problems in which the coarse cells are not optically thick, this logic is valid, as we show below.

III. THE LINEARIZED COARSE-MESH FINITE DIFFERENCE METHOD

To describe the linearization procedure, we consider the transport problem defined by Eqs. (2), with

$$q_j = \sigma_{a,j}\Lambda + \varepsilon\tilde{q}_j \ , \tag{25a}$$

$$\psi_n^b = \frac{\Lambda}{2} + \varepsilon\tilde{\psi}_n^b \ , \tag{25b}$$

where Λ is an arbitrary constant and $\varepsilon \ll 1$. For $\varepsilon = 0$, the resulting problem has the exact flat solution

$$\psi_{n,j} = \psi_{n,j+1/2} = \frac{\Lambda}{2} \ .$$

If we set

$$\psi_{n,j} = \frac{\Lambda}{2} + \varepsilon\tilde{\psi}_{n,j} \ , \tag{26a}$$

$$\psi_{n,j+1/2} = \frac{\Lambda}{2} + \varepsilon\tilde{\psi}_{n,j+1/2} \ , \tag{26b}$$

then Eqs. (2) for $\psi_{n,j}$ and $\psi_{n,j+1/2}$ easily become

$$\frac{\mu_n}{h_j}\left(\tilde{\psi}_{n,j+1/2} - \tilde{\psi}_{n,j+1/2}\right) + \sigma_{t,j}\tilde{\psi}_{n,j} = \frac{\sigma_{s,j}}{2}\sum_{m=1}^{N}\tilde{\psi}_{m,j}w_m + \frac{\tilde{q}_j}{2} \ , \tag{27a}$$

$$\tilde{\psi}_{n,j} = \left(\frac{1+\alpha_{n,j}}{2}\right)\tilde{\psi}_{n,j+1/2} + \left(\frac{1-\alpha_{n,j}}{2}\right)\tilde{\psi}_{n,j-1/2} \ , \tag{27b}$$

$$\tilde{\psi}_{n,1/2} = \tilde{\psi}_n^b \ , \ \mu_n > 0 \ , \tag{27c}$$

$$\tilde{\psi}_{n,J+1/2} = \tilde{\psi}_n^b \ , \ \mu_n < 0 \ . \tag{27d}$$

These equations are identical to Eqs. (2), except that ψ and q have been replaced by $\tilde{\psi}$ and $\tilde{q}$. [Of course, this happens because Eqs. (2) are linear.]

Because the CMDSA method is linear, the CMDSA equations obtained by introducing Eqs. (25) and (26) are also the same as the original equations, but with the ψ's, ϕ's, and q's replaced by $\tilde{\psi}$'s, $\tilde{\phi}$'s, and $\tilde{q}$'s. Explicitly, the fine-mesh transport sweep Eqs. (5) become

$$\frac{\mu_n}{h_j}\left(\tilde{\psi}_{n,j+1/2}^{(\ell+1/2)} - \tilde{\psi}_{n,j-1/2}^{(\ell+1/2)}\right) + \sigma_{t,j}\tilde{\psi}_{n,j}^{(\ell+1/2)} = \frac{\sigma_{s,j}}{2}\tilde{\phi}_{0,j}^{(\ell)} + \frac{\tilde{q}_j}{2} \ , \tag{28a}$$

$$\tilde{\psi}_{n,j}^{(\ell+1/2)} = \left(\frac{1+\alpha_{n,j}}{2}\right)\tilde{\psi}_{n,j+1/2}^{(\ell+1/2)} + \left(\frac{1-\alpha_{n,j}}{2}\right)\tilde{\psi}_{n,j-1/2}^{(\ell+1/2)} \ , \tag{28b}$$

$$\tilde{\psi}_{n,1/2}^{(\ell+1/2)} = \tilde{\psi}_n^b \ , \ \mu_n > 0 \ , \tag{28c}$$

$$\tilde{\psi}_{n,J+1/2}^{(\ell+1/2)} = \tilde{\psi}_n^b \ , \ \mu_n < 0 \ . \tag{28d}$$

The updated scalar fluxes are

$$\tilde{\phi}_{0,j}^{(\ell+1/2)} = \sum_{n=1}^{N}\tilde{\psi}_{n,j}^{(\ell+1/2)}w_n \ . \tag{29}$$

The low-order coarse-grid diffusion Eqs. (22) (with $\tilde{F} = \varepsilon F$) become

$$\tilde{F}_{1,k+1/2}^{(\ell+1)} - \tilde{F}_{1,k-1/2}^{(\ell+1)} + \Sigma_{a,k}\tilde{F}_{0,k}^{(\ell+1)}\Delta_k = \sum_{j\in k}\sigma_{s,j}\left(\tilde{\phi}_{0,j}^{(\ell+1/2)} - \tilde{\phi}_{0,j}^{(\ell)}\right)h_j \ , \ 1 \le k \le K \ , \tag{30a}$$

$$\tilde{F}_{1,k+1/2}^{(\ell+1)} = -\frac{2}{3}\left(\frac{\tilde{F}_{0,k+1}^{(\ell+1)} - \tilde{F}_{0,k}^{(\ell+1)}}{\Sigma_{t,k+1}\Delta_{k+1} + \Sigma_{t,k}\Delta_k}\right) \ , \quad 1 \le k \le K-1 \ , \tag{30b}$$

$$0 = \tilde{F}_{1,1/2}^{(\ell+1)} + \beta\tilde{F}_{0.1}^{(\ell+1)} \ , \tag{30c}$$

$$0 = -\tilde{F}_{1,K+1/2}^{(\ell+1)} + \beta\tilde{F}_{0,K}^{(\ell+1)} \ . \tag{30d}$$

The fine-grid accelerated scalar flux Eq. (24) becomes

$$\tilde{\phi}_{0,j}^{(\ell+1)} = \tilde{\phi}_{0,j}^{(\ell+1/2)} + \tilde{F}_{0,k}^{(\ell+1)} \ , \quad j \in k \ , \quad 1 \le k \le K \ . \tag{31}$$

To repeat, these equations are identical to the original equations, except that all quantities scaled by ε now have a tilde. This occurs because, like the original transport problem, the CMDSA equations are linear.

The CMFD method, however, is nonlinear; this method is altered when Eqs. (25) and (26) are introduced and the resulting equations are expanded in powers of ε. For the CMFD method, the fine-mesh transport sweep and the resulting updated scalar flux equations are the same as with CMDSA and are described by Eqs. (28) and (29).

However, introducing Eqs. (25) and (26) into (16) and expanding in ε, we obtain a different set of low-order diffusion equations for $\tilde{\Phi}_{0,k}^{(\ell+1)}$. A key identity is

$$\Sigma_{a,k}^{(\ell+1/2)}\Phi_{0,k}^{(\ell+1)}$$

$$=\frac{\sum_{j\in k}\sigma_{a,j}\left(\Lambda+\varepsilon\tilde{\phi}_{0,j}^{(\ell+1/2)}\right)h_j}{\sum_{j\in k}\left(\Lambda+\varepsilon\tilde{\phi}_{0,j}^{(\ell+1/2)}\right)h_j}\left[\Lambda+\varepsilon\tilde{\Phi}_{0,k}^{(\ell+1)}\right]$$

$$=\frac{\Lambda\Sigma_{a,k}\Delta_k+\varepsilon\sum_{j\in k}\sigma_{a,j}\tilde{\phi}_{0,j}^{(\ell+1/2)}h_j}{\Lambda\Delta_k+\varepsilon\sum_{j\in k}\tilde{\phi}_{0,j}^{(\ell+1/2)}h_j}\left[\Lambda+\varepsilon\tilde{\Phi}_{0,k}^{(\ell+1)}\right]$$

$$=\cdots$$

$$=\Sigma_{a,k}\Lambda+\varepsilon\left[\frac{1}{\Delta_k}\sum_{j\in k}(\sigma_{a,j}-\Sigma_{a,k})\tilde{\phi}_{0,j}^{(\ell+1/2)}h_j+\Sigma_{a,k}\tilde{\Phi}_{0,k}^{(\ell+1)}\right]. \tag{32}$$

Thus, Eq. (16a) becomes

$$\begin{aligned}&\varepsilon\tilde{\Phi}_{1,k+1/2}^{(\ell+1)}-\varepsilon\tilde{\Phi}_{1,k-1/2}^{(\ell+1)}+\Sigma_{a,k}\Lambda\Delta_k\\&+\varepsilon\left[\sum_{j\in k}(\sigma_{a,j}-\Sigma_{a,k})\tilde{\phi}_{0,j}^{(\ell+1/2)}h_j+\Sigma_{a,k}\tilde{\Phi}_{0,k}^{(\ell+1)}\Delta_k\right]\\&=\sum_{j\in k}(\sigma_{a,j}\Lambda+\varepsilon\tilde{q}_j)h_j=(\Sigma_{a,k}\Lambda+\varepsilon\tilde{Q}_k)\Delta_k,\end{aligned}$$

or,

$$\begin{aligned}\tilde{\Phi}_{1,k+1/2}^{(\ell+1)}-\tilde{\Phi}_{1,k-1/2}^{(\ell+1)}+\Sigma_{a,k}\tilde{\Phi}_{0,k}^{(\ell+1)}\Delta_k\\=\tilde{Q}_k\Delta_k+\sum_{j\in k}(\Sigma_{a,k}-\sigma_{a,j})\tilde{\phi}_{0,j}^{(\ell+1/2)}h_j\ .\end{aligned} \tag{33}$$

Next, Eq. (14) for $\hat{D}_{k+1/2}^{(\ell+1/2)}$ yields

$$\begin{aligned}\varepsilon\tilde{\Phi}_{1,k+1/2}^{(\ell+1/2)}=-\frac{2}{3}\left(\frac{\varepsilon(\tilde{\Phi}_{0,k+1}^{(\ell+1/2)}-\tilde{\Phi}_{0,k}^{(\ell+1/2)})}{\Sigma_{t,k+1}\Delta_{k+1}+\Sigma_{t,k}\Delta_k+O(\varepsilon)}\right)\\+\hat{D}_{k+1/2}^{(\ell+1/2)}(2\Lambda+O(\varepsilon)),\end{aligned}$$

or,

$$\hat{D}_{k+1/2}^{(\ell+1/2)}=\frac{\varepsilon}{2\Lambda}\left[\tilde{\Phi}_{1,k+1/2}^{(\ell+1/2)}+\frac{2}{3}\left(\frac{\tilde{\Phi}_{0,k+1}^{(\ell+1/2)}-\tilde{\Phi}_{0,k}^{(\ell+1/2)}}{\Sigma_{t,k+1}\Delta_{k+1}+\Sigma_{t,k}\Delta_k}\right)\right]+O(\varepsilon^2)\ . \tag{34}$$

Using this result in Eq. (16b), we obtain for $1\le k\le K-1$:

$$\begin{aligned}\tilde{\Phi}_{1,k+1/2}^{(\ell+1)}=-\frac{2}{3}\left(\frac{\tilde{\Phi}_{0,k+1}^{(\ell+1)}-\tilde{\Phi}_{0,k}^{(\ell+1)}}{\Sigma_{t,k+1}\Delta_{k+1}+\Sigma_{t,k}\Delta_k}\right)\\+\tilde{\Phi}_{1,k+1/2}^{(\ell+1/2)}+\frac{2}{3}\left(\frac{\tilde{\Phi}_{0,k+1}^{(\ell+1/2)}-\tilde{\Phi}_{0,k}^{(\ell+1/2)}}{\Sigma_{t,k+1}\Delta_{k+1}+\Sigma_{t,k}\Delta_k}\right).\end{aligned} \tag{35}$$

Next, introducing Eqs. (25) and (26) into Eq. (16c), we get

$$\begin{aligned}2\sum_{\mu_n>0}\mu_n\left(\frac{\Lambda}{2}+\varepsilon\tilde{\psi}_n^b\right)w_n\\=\varepsilon\tilde{\Phi}_{1,1/2}^{(\ell+1)}+\frac{\sum_{n=1}^{N}|\mu_n|\left(\frac{\Lambda}{2}+\varepsilon\tilde{\psi}_{n,1/2}^{(\ell+1/2)}\right)w_n}{\Lambda+\varepsilon\tilde{\Phi}_{0,1}^{(\ell+1/2)}}\\\times\left(\Lambda+\varepsilon\tilde{\Phi}_{0,1}^{(\ell+1)}\right).\end{aligned}$$

Expanding this equation in ε and discarding the $O(\varepsilon^2)$ terms, we obtain

$$\tilde{\Phi}_{1,1/2}^{(\ell+1)}+\beta\tilde{\Phi}_{0,1}^{(\ell+1)}=\tilde{\Phi}_{1,1/2}^{(\ell+1/2)}+\beta\tilde{\Phi}_{0,1}^{(\ell+1/2)}\ . \tag{36a}$$

At the right edge of the system, a similar result holds:

$$-\tilde{\Phi}_{1,K+1/2}^{(\ell+1)}+\beta\tilde{\Phi}_{0,J}^{(\ell+1)}=-\tilde{\Phi}_{1,K+1/2}^{(\ell+1/2)}+\beta\tilde{\Phi}_{0,K}^{(\ell+1/2)}\ . \tag{36b}$$

Finally, the fine-grid acceleration Eq. (17) becomes, for $j\in k$,

$$\Lambda+\varepsilon\tilde{\phi}_{0,j}^{(\ell+1)}=\left(\Lambda+\varepsilon\tilde{\phi}_{0,j}^{(\ell+1/2)}\right)\left(\frac{\Lambda+\varepsilon\tilde{\Phi}_{0,k}^{(\ell+1)}}{\Lambda+\varepsilon\tilde{\Phi}_{0,k}^{(\ell+1/2)}}\right). \tag{37}$$

Expanding in powers of ε and dropping terms of $O(\varepsilon^2)$, we get

$$\tilde{\phi}_{0,j}^{(\ell+1)}=\tilde{\phi}_{0,j}^{(\ell+1/2)}+(\tilde{\Phi}_{0,k}^{(\ell+1)}-\tilde{\Phi}_{0,k}^{(\ell+1/2)})\ ,\ j\in k\ ,\ 1\le k\le K\ . \tag{38}$$

Thus, the LCMFD method is defined by

1. transport sweep: Eqs. (28)
2. updated scalar flux: Eq. (29)
3. low-order coarse-grid diffusion: Eqs. (33), (35), and (36)
4. accelerated fine-grid scalar fluxes: Eq. (38)

The first two (transport sweep) steps [Eqs. (28) and (29)] are identical for the CMDSA and LCMFD methods. To establish the connection between the acceleration steps of the two methods, we shall show that

$$\tilde{F}_{0,k}^{(\ell+1)} = \tilde{\Phi}_{0,k}^{(\ell+1)} - \tilde{\Phi}_{0,k}^{(\ell+1/2)} , \tag{39a}$$

$$\tilde{F}_{1,k+1/2}^{(\ell+1)} = \tilde{\Phi}_{1,k+1/2}^{(\ell+1)} - \tilde{\Phi}_{1,k+1/2}^{(\ell+1/2)} . \tag{39b}$$

More precisely, the low-order CMDSA Eqs. (22) and (24) are defined for $\tilde{F}_{0,k}^{(\ell+1)}$ and $\tilde{F}_{1,k+1/2}^{(\ell+1)}$, while the low-order LCMFD Eqs. (33), (35), (36), and (38) are defined for $\tilde{\Phi}_{0,k}^{(\ell+1)}$ and $\tilde{\Phi}_{1,k+1/2}^{(\ell+1)}$. We use Eqs. (39) to show that the LCMFD low-order acceleration equations are algebraically equivalent to the CMDSA low-order acceleration equations.

At the end of a transport sweep, Eq. (28a) holds, so

$$\frac{1}{h_j}\left(\tilde{\phi}_{1,j+1/2}^{(\ell+1/2)} - \tilde{\phi}_{1,j-1/2}^{(\ell+1/2)}\right) + \sigma_{t,j}\tilde{\phi}_{0,j}^{(\ell+1/2)} = \sigma_{s,j}\tilde{\phi}_{0,j}^{(\ell)} + \tilde{q}_j .$$

Equivalently,

$$\begin{aligned}\frac{1}{h_j}\left(\tilde{\phi}_{1,j+1/2}^{(\ell+1/2)} - \tilde{\phi}_{1,j-1/2}^{(\ell+1/2)}\right) + \Sigma_{a,k}\tilde{\phi}_{0,j}^{(\ell+1/2)} \\ = \sigma_{s,j}\left(\tilde{\phi}_{0,j}^{(\ell)} - \tilde{\phi}_{0,j}^{(\ell+1/2)}\right) + \tilde{q}_j + \left(\Sigma_{a,k} - \sigma_{a,j}\right)\tilde{\phi}_{0,j}^{(\ell+1/2)} .\end{aligned} \tag{40}$$

Operating by $\sum_{j\in k}(\cdot)h_j$, we obtain

$$\begin{aligned}\tilde{\Phi}_{1,k+1/2}^{(\ell+1/2)} - \tilde{\Phi}_{1,k-1/2}^{(\ell+1/2)} + \Sigma_{a,k}\tilde{\Phi}_{0,k}^{(\ell+1/2)}\Delta_k \\ = \sum_{j\in k}\sigma_{s,j}\left(\tilde{\phi}_{0,j}^{(\ell)} - \tilde{\phi}_{0,j}^{(\ell+1/2)}\right)h_j \\ + \tilde{Q}_k\Delta_k + \sum_{j\in k}\left(\Sigma_{a,k} - \sigma_{a,j}\right)\tilde{\phi}_{0,j}^{(\ell+1/2)}h_j .\end{aligned} \tag{41}$$

Subtracting this result from the LCMFD balance Eq. (33) and using the definitions (39), we obtain

$$\begin{aligned}\tilde{F}_{1,k+1/2}^{(\ell+1)} - \tilde{F}_{1,k-1/2}^{(\ell+1)} + \Sigma_{a,k}\tilde{F}_{0,k}^{(\ell+1)}\Delta_k \\ = \sum_{j\in k}\sigma_{s,j}\left(\tilde{\phi}_{0,j}^{(\ell+1/2)} - \tilde{\phi}_{0,j}^{(\ell)}\right)h_j .\end{aligned} \tag{42}$$

This is the CMDSA balance Eq. (30a).

Next, Eqs. (35) and (39) immediately give

$$\tilde{F}_{1,k+1/2}^{(\ell+1)} = -\frac{2}{3}\left(\frac{\tilde{F}_{0,k+1/2}^{(\ell+1)} - \tilde{F}_{0,k}^{(\ell+1)}}{\Sigma_{t,k+1}\Delta_{k+1} + \Sigma_{t,k}\Delta_k}\right) . \tag{43}$$

This is the CMDSA Fick's Law, Eq. (30b).

Next, Eqs. (36) and (39) immediately give

$$0 = \tilde{F}_{1,1/2}^{(\ell+1)} + \beta\tilde{F}_{0,1}^{(\ell+1)} , \tag{44a}$$

$$0 = -\tilde{F}_{1,K+1/2}^{(\ell+1)} + \beta\tilde{F}_{0,K}^{(\ell+1)} . \tag{44b}$$

These are the CMDSA boundary conditions, Eqs. (30c) and (30d).

Finally, Eqs. (38) and (39) become

$$\tilde{\phi}_{0,j}^{(\ell+1)} = \tilde{\phi}_{0,j}^{(\ell+1/2)} + \tilde{F}_{0,k}^{(\ell+1)} , \quad j\in k , \quad 1\le k\le K . \tag{45}$$

This is the CMDSA acceleration Eq. (31).

These results show that *the CMDSA and LCMFD methods are algebraically equivalent.*

Remarks:

1. In previous publications, linearizations of nonlinear transport acceleration methods were derived only for homogeneous systems with flat sources and uniform grids.[8,11–14] In the more general linearization performed in this paper, the physical system does not need to be homogeneous, the sources do not need to be flat, and the spatial grid does not need to be uniform. Thus, the linearization in this paper establishes a much broader theoretical link between the nonlinear CMFD and the linear CMDSA methods—these methods are essentially equivalent over a larger class of problems. (However, the restriction to a homogeneous system with a uniform spatial grid is necessary for the Fourier analysis presented in Sec. IV.)

2. The linearization defined by Eqs. (25) and (26) uses that for $\varepsilon = 0$, the transport problem with the internal source and boundary conditions

$$q_j = \sigma_{a,j}\Lambda \quad , \quad \psi_n^b = \frac{\Lambda}{2} , \tag{46a}$$

has the *constant* solution

$$\psi_{n,j} = \psi_{n+1/2,j} = \frac{\Lambda}{2} . \tag{46b}$$

This special solution is the one around which the CMFD method is linearized. The internal and boundary forces Eq. (46a) that lead to this solution were derived by the method of manufactured solutions; i.e., assume Eq. (46b), and then the discrete transport equations yield Eq. (46a).

3. The details of the CMDSA discretization method discussed in this paper were chosen to match exactly the linearized CMFD discretization method. However, there are alternative choices in how these discretizations can be done, particularly in the choice of boundary conditions, and these choices determine whether there is exact algebraic equivalence between the LCMFD and CMDSA methods. The main result of this paper is that for any specific choice of a CMFD method, the linearization of this method (in the manner

shown in this paper) is algebraically equivalent to a specific CMDSA method.

IV. FOURIER ANALYSIS

To perform the Fourier analysis, the equations of CMDSA/LCMFD are simplified by assuming an infinite homogeneous medium with a uniform spatial grid and a specified number p of fine cells per coarse cell:

$$\mu_n\left(\psi_{n,j+1/2}^{(\ell+1/2)}-\psi_{n,j-1/2}^{(\ell+1/2)}\right)+\sigma_t h\psi_{n,j}^{(\ell+1/2)}=\frac{c\sigma_t h}{2}\phi_{0,j}^{(\ell)}+\frac{q_j}{2}\ , \tag{47a}$$

$$\psi_{n,j}^{(\ell+1/2)}=\frac{1+\alpha_n}{2}\psi_{n,j+1/2}^{(\ell+1/2)}+\frac{1-\alpha_n}{2}\psi_{n,j-1/2}^{(\ell+1/2)}\ , \tag{47b}$$

$$-\frac{1}{3p\sigma_t h}\left(F_{0,k+1}^{(\ell+1)}-2F_{0,k}^{(\ell+1)}+F_{0,k-1}^{(\ell+1)}\right)+(1-c)p\sigma_t hF_{0,k}^{(\ell+1)}=c\sigma_t h\sum_{j\in k}\left(\phi_{0,j}^{(\ell+1/2)}-\phi_{0,j}^{(\ell)}\right)\ , \tag{47c}$$

$$\phi_{0,j}^{(\ell+1)}=\phi_{0,j}^{(\ell+1/2)}+F_{0,k}^{(\ell+1/2)},\qquad j\in k\ . \tag{47d}$$

We choose the following ansatz, which eliminates aliasing between the fine-cell and coarse-cell modes and results in a system of equations with substantially fewer exponential terms. Let j' denote the (integer) label for any cell in the infinite system, $-\infty<j'<\infty$. Also, let j be a positive integer satisfying $1\le j\le p$, and let k be an integer such that

$$j'=(k-1)p+j\ .$$

Then, for each j', j and k are unique, k labels the coarse cell within which cell j' resides, and j labels the position within coarse cell k at which fine cell j' resides. The Fourier ansatz can now be stated as

$$q_j=0\ ,$$

$$\psi_{n,j'-1/2}^{(\ell+1/2)}=\omega^\ell d_{n,j}e^{i\lambda\sigma_t x_k}\ ,$$

$$\psi_{n,j'}^{(\ell+1/2)}=\omega^\ell a_{n,j}e^{i\lambda\sigma_t x_k}\ ,$$

$$\phi_{0,j'}^{(\ell)}=\omega^\ell g_j e^{i\lambda\sigma_t x_k}\ ,$$

$$F_{0,k}^{(\ell+1)}=\omega^\ell F e^{i\lambda\sigma_t x_k}\ .$$

Inserting this ansatz into Eqs. (47), we obtain

$$\begin{aligned}&\mu_n\left(d_{n,j+1}-d_{n,j}\right)+\sigma_t h a_{n,j}=\tfrac{c\sigma_t h}{2}g_j,\qquad 1\le j\le p-1\ ,\\ &\mu_n\left(d_{n,1}e^{i\lambda P\sigma_t h}-d_{n,j}\right)+\sigma_t h a_{n,j}=\tfrac{c\sigma_t h}{2}g_j,\quad j=p\ ,\end{aligned} \tag{48a}$$

$$\begin{aligned}&a_{n,j}=\tfrac{1+\alpha_n}{2}d_{n,j+1}+\tfrac{1-\alpha_n}{2}d_{n,j},\qquad 1\le j\le p-1\ ,\\ &a_{n,j}=\tfrac{1+\alpha_n}{2}d_{n,1}e^{i\lambda p\sigma_t h}+\tfrac{1-\alpha_n}{2}d_{n,j},\quad j=p\ ,\end{aligned} \tag{48b}$$

$$-\frac{F}{3p\sigma_t h}\left(e^{i\lambda p\sigma_t h}-2+e^{-i\lambda p\sigma_t h}\right)+(1-c)p\sigma_t hF=c\sigma_t h\sum_{j=1}^{p}\left(\sum_{n=1}^{N}w_n a_{n,j}-g_j\right)\ , \tag{48c}$$

$$\omega g_j=\sum_{n=1}^{N}w_n a_{n,j}+F\ . \tag{48d}$$

Equations (48c) and (48d) can be combined, yielding

$$\begin{aligned}&a_{n,j}+\frac{\mu_n}{\sigma_t h}d_{n,j+1}-\frac{\mu_n}{\sigma_t h}d_{n,j}-\frac{c}{2}g_j=0\ ,\qquad 1\le j\le p-1\ ,\\ &a_{n,j}+\left(\frac{\mu_n}{\sigma_t h}e^{i\lambda p\sigma_t h}\right)d_{n,1}-\frac{\mu_n}{\sigma_t h}d_{n,j}-\frac{c}{2}g_j=0\ ,\quad j=p\ ,\end{aligned} \tag{49a}$$

$$\begin{aligned}&a_{n,j}-\frac{1+\alpha_n}{2}d_{n,j+1}-\frac{1-\alpha_n}{2}d_{n,j}=0\ ,\qquad 1\le j\le p-1\ ,\\ &a_{n,j}-\left(\frac{1+\alpha_n}{2}e^{i\lambda p\sigma_t h}\right)d_{n,1}-\frac{1-\alpha_n}{2}d_{n,j}=0\ ,\quad j=p\ ,\end{aligned} \tag{49b}$$

$$\sum_{n=1}^{N}w_n\left(a_{n,j}+\hat{F}\sum_{j'=1}^{p}a_{n,j'}\right)-\hat{F}\sum_{j'=1}^{p}g_{j'}-\omega g_j=0\ , \tag{49c}$$

$$\hat{F}=\frac{c\sigma_t h}{\frac{2}{3p\sigma_t h}\left[1-\cos(\lambda p\sigma_t h)\right]+(1-c)p\sigma_t h}\ .$$

Representing this system of Eqs. (49) in block matrix form, we obtain

$$\begin{bmatrix}\mathbf{A} & \mathbf{B}\\ \mathbf{C} & \mathbf{D}-\omega\mathbf{I}\end{bmatrix}\begin{bmatrix}\mathbf{f}\\ \mathbf{g}\end{bmatrix}=\begin{bmatrix}0\\ 0\end{bmatrix}\ . \tag{50}$$

Here, the entries of the $2Np \times 2Np$ matrix $\mathbf{A}$ are the coefficients of $a_{n,j}$ and $d_{n,j}$ in Eqs. (49a) and (49b). The entries of the $2Np \times p$ matrix $\mathbf{B}$ are the coefficients of g_j in Eqs. (49a) and (49b). The entries of the $p \times 2Np$ matrix $\mathbf{C}$ are the coefficients of $a_{n,j}$ in Eq. (49c). The entries of the $p \times p$ matrix $\mathbf{D}$ are the coefficients of g_j in Eq. (49c). The entries of the $2Np$ column vector $\mathbf{f}$ are the terms $a_{n,j}$ and $d_{n,j}$. The entries of the p column vector $\mathbf{g}$ are the terms g_j.

The block matrix can be decomposed as follows:

$$\begin{bmatrix} \mathbf{A} & \mathbf{B} \\ \mathbf{C} & \mathbf{D}-\omega\mathbf{I} \end{bmatrix} = \begin{bmatrix} \mathbf{A} & 0 \\ \mathbf{C} & \mathbf{I} \end{bmatrix} \begin{bmatrix} \mathbf{I} & \mathbf{A}^{-1}\mathbf{B} \\ 0 & \mathbf{D}-\mathbf{C}\mathbf{A}^{-1}\mathbf{B}-\omega\mathbf{I} \end{bmatrix} . \quad (51)$$

The determinant of the original matrix can then be found via

$$\begin{aligned} \begin{vmatrix} \mathbf{A} & \mathbf{B} \\ \mathbf{C} & \mathbf{D}-\omega\mathbf{I} \end{vmatrix} &= \begin{vmatrix} \mathbf{A} & 0 \\ \mathbf{C} & \mathbf{I} \end{vmatrix} \begin{vmatrix} \mathbf{I} & \mathbf{A}^{-1}\mathbf{B} \\ 0 & \mathbf{D}-\mathbf{C}\mathbf{A}^{-1}\mathbf{B}-\omega\mathbf{I} \end{vmatrix} \\ &= |\mathbf{A}| \left| \mathbf{D}-\mathbf{C}\mathbf{A}^{-1}\mathbf{B}-\omega\mathbf{I} \right| . \end{aligned} \quad (52)$$

From Eq. (50), we know that $\begin{vmatrix} \mathbf{A} & \mathbf{B} \\ \mathbf{C} & \mathbf{D}-\omega\mathbf{I} \end{vmatrix} = 0$. Also, from inspection of Eqs. (49a) and (49b), we know that the rows of matrix $\mathbf{A}$ are linearly independent, implying $|\mathbf{A}| \neq 0$. Therefore,

$$|\mathbf{D}-\mathbf{C}\mathbf{A}^{-1}\mathbf{B}-\omega\mathbf{I}| = 0 , \quad (53)$$

and thus, ω_j, $1 \leq j \leq p$, are the eigenvalues of the $p \times p$ matrix $\mathbf{D}-\mathbf{C}\mathbf{A}^{-1}\mathbf{B}$. We compute these eigenvalues numerically as functions of λ, and then we calculate the spectral radius:

$$\rho = \sup_{\lambda} \sup_{1 \leq j \leq p} \left| \omega_j(\lambda) \right| . \quad (54)$$

V. NUMERICAL RESULTS

The spectral radius is predicted theoretically by the Fourier analysis described above. To confirm that the behavior of CMFD and CMDSA matches this analysis, we estimate the spectral radii of these methods experimentally. The problem used to estimate the spectral radius of the CMDSA method consists of a system with a vacuum boundary on the left side of the slab and a reflecting boundary on the right side with no interior source. The solution of this problem is zero throughout the system, and we initialize the iterative CMDSA method with a step function and observe its convergence to the zero solution. (By choosing a step function as our initial guess, we seed the system with all Fourier modes.) For this problem, the spectral radius can be measured as

$$\rho = \frac{\left|\left| \phi^{(\ell+1)} \right|\right|}{\left|\left| \phi^{(\ell)} \right|\right|} . \quad (55)$$

This problem cannot be used to estimate the spectral radius of CMFD, because the lack of an interior and boundary source causes the low-order problem to produce the exact zero solution in a single iteration. Instead, we choose the same boundary conditions but with a step function source within the system. The CMFD spectral radius can then be estimated as

$$\rho = \frac{\left|\left| \phi^{(\ell+1)} - \phi^{(\ell)} \right|\right|}{\left|\left| \phi^{(\ell)} - \phi^{(\ell-1)} \right|\right|} . \quad (56)$$

Figures 2 through 17 show comparisons between the experimental results of these two methods for various coarse-cell optical thicknesses, scattering ratios, and numbers of fine cells per coarse cell.

First, Figs. 2 through 5 describe *fine-mesh acceleration* (each coarse spatial cell contains $p = 1$ fine spatial cell). In this case, the CMDSA method is the same as the standard fine-mesh DSA method. For small scattering ratios c, the CMDSA and CMFD methods are seen to be stable for all spatial cells and efficient for most spatial cells. However, as c increases, the methods are stable and efficient for cells less than approximately 1 mfp thick but become unstable for cells greater than approximately 2 mfp thick. The CMDSA and CMFD methods have almost identical spectral radii, and the agreement between theory (Fourier analysis) and experiment (numerical simulation) is excellent.

Next, Figs. 6 through 9 describe *coarse-mesh acceleration* in which each coarse spatial cell contains $p = 2$ fine-mesh cells. Qualitatively, the results are similar to fine-mesh acceleration: the CMDSA and CMFD methods are stable and efficient for coarse spatial cells less than approximately 1 mfp thick, but for scattering ratios near unity, the methods become unstable for coarse spatial cells greater than approximately 2 mfp thick. The $p = 2$ spectral radii are higher than the $p = 1$ spectral radii, as should be expected, because the same coarse-mesh calculation is now being asked to accelerate twice as many fine-mesh unknowns. As before, the CMDSA and CMFD methods have almost the same spectral radii, and the agreement between theory and experiment is excellent.

Figures 10 through 13 describe coarse-mesh acceleration with $p = 3$ fine cells per coarse cell. The results here are qualitatively similar to the $p = 2$ results. The $p = 3$ spectral radii are higher than the $p = 2$ spectral radii, as expected from the reasons noted previously. Also, as in the previous simulations, the agreement between theory and experiment is excellent.

Finally, Figs. 14 through 17 describe coarse-mesh acceleration with $p = 4$ fine cells per coarse spatial cell.

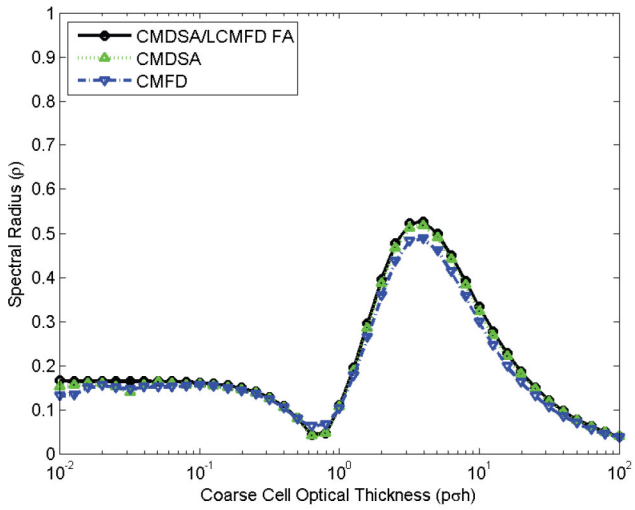

Fig. 2. Spectral radius for $p=1$ and $c=0.8$.

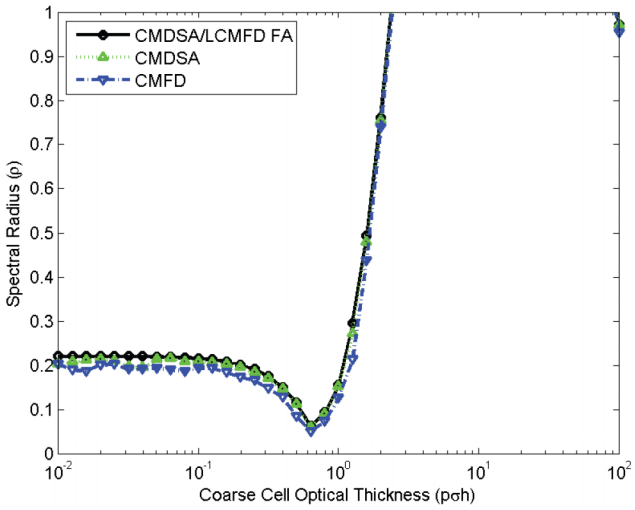

Fig. 4. Spectral radius for $p=1$ and $c=0.99$.

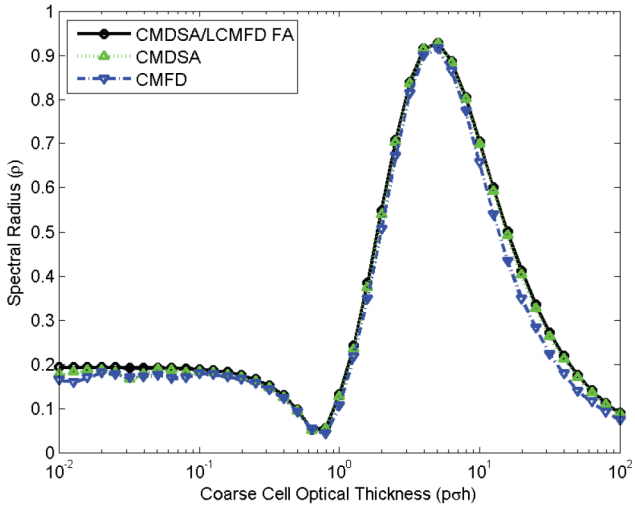

Fig. 3. Spectral radius for $p=1$ and $c=0.9$.

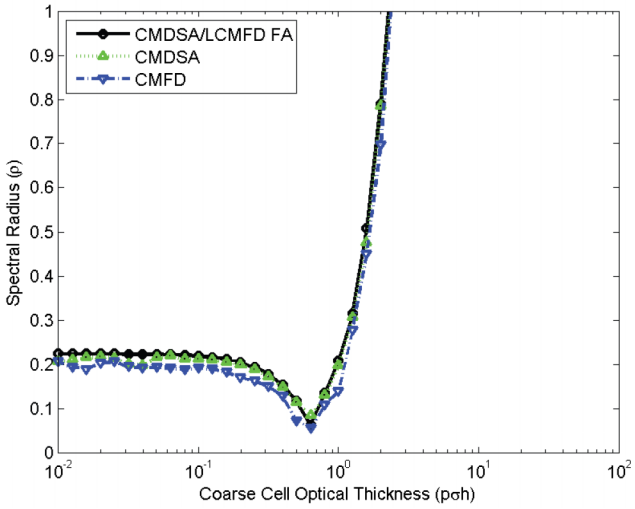

Fig. 5. Spectral radius for $p=1$ and $c=0.9999$.

All the trends noted previously are continued in these figures, including the excellent agreement between theory and experiment.

In Figs. 2 through 17, the Fourier analysis yields an upper bound to the spectral radius. This is because the experimental neutron systems are finite, and neutron leakage from these systems reduces the theoretical (infinite medium) spectral radius slightly. Also, the spectral radius describes the asymptotic trend of the method after many iterations. Thus, small spectral radii ρ can be difficult to measure experimentally, as the solution converges so rapidly that roundoff error can present itself before a good estimate of ρ is achieved. [This issue is most significant with our estimates of the CMFD ρ using Eq. (56), which is more sensitive to roundoff errors than Eq. (55). In particular, for small ρ the measured CMFD ρ are often slightly lower than the Fourier analysis predictions. The likely reason for this is that the CMFD numerical experiments could not be run to a sufficiently large number of iterations.]

A somewhat surprising result of our experiments is that although the CMDSA calculations are performed with volume-weighted cross sections, and the CMFD calculations are performed with flux-weighted cross sections, the two calculations yield almost identical results—even for problems in which the scalar flux is not nearly constant. At this time we cannot offer a mathematical explanation for this experimental observation.

We also note that the general shape of Figs. 2 through 5 ($p=1$) differs substantially from that of Figs. 6 through

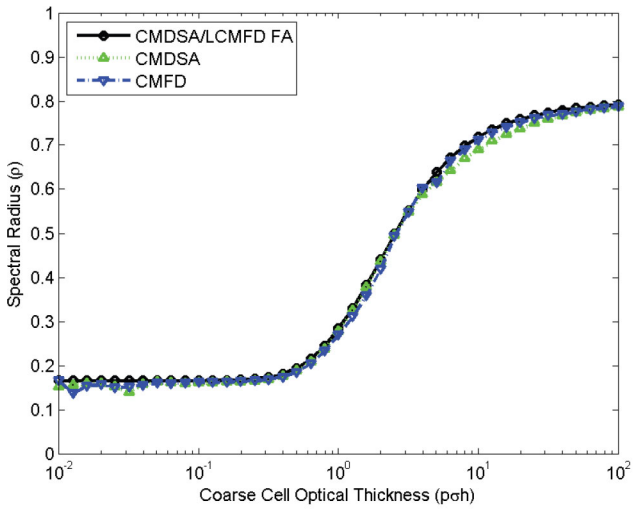

Fig. 6. Spectral radius for $p=2$ and $c=0.8$.

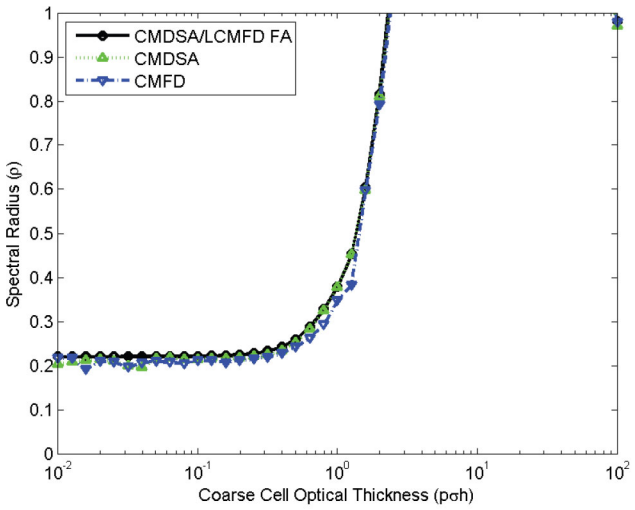

Fig. 8. Spectral radius for $p=2$ and $c=0.99$.

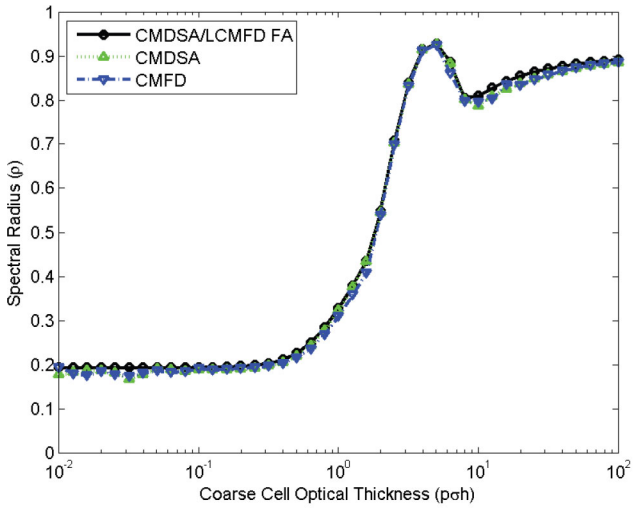

Fig. 7. Spectral radius for $p=2$ and $c=0.9$.

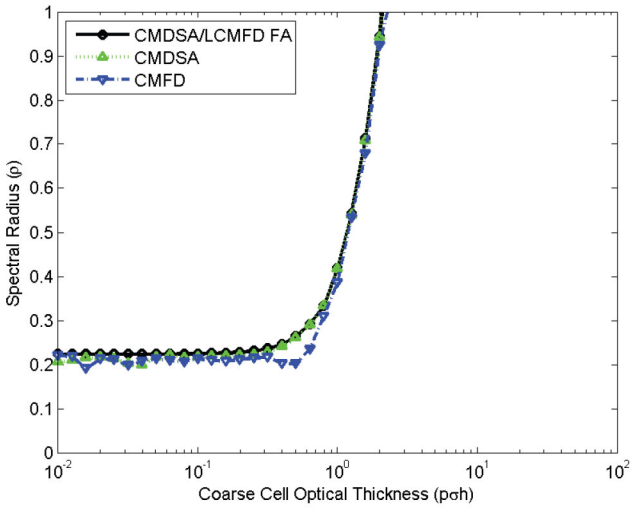

Fig. 9. Spectral radius for $p=2$ and $c=0.9999$.

17 ($p\geq 2$). Presumably, the reason for this is that for $p=1$, the low-order solution only needs to account for the difference between the transport and diffusion solutions on the same spatial grid. However, for $p\geq 2$, the low-order solution also must deal with the discrepancy that the diffusion equation is discretized on a coarser spatial grid.

Finally, we note that the numerical results shown above are consistent with the CMFD results obtained previously by Cho and Park.[8]

VI. CONCLUSIONS

We have derived—and demonstrated numerically—a close theoretical relationship between the DSA and CMFD methods for accelerating the iterative convergence of particle transport calculations. These two methods were developed independently and have been used for many years in production neutron transport codes.

To the reader who is familiar with the history of DSA and the long (and only partly successful) effort to derive unconditionally stable versions of this method for specified transport discretization schemes, a natural question is, if CMFD is stable only for spatial cells less than approximately 2 mfp thick, then how could this method be used successfully in practical problems? The answer seems to have two parts:

1. In practical multigroup reactor core simulations, CMFD is observed to be somewhat more stable than for

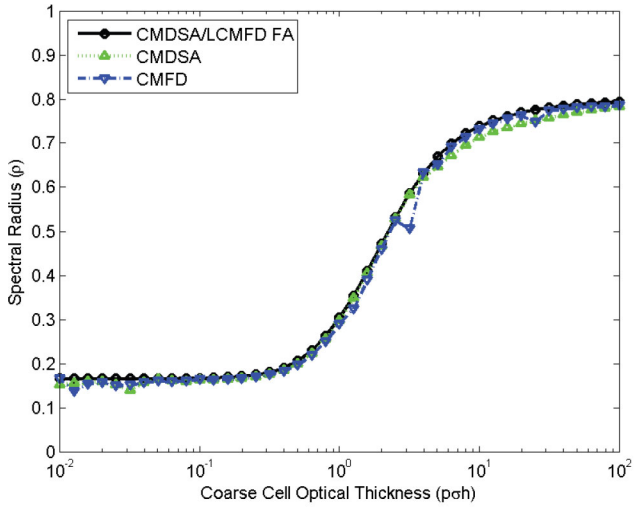

Fig. 10. Spectral radius for $p=3$ and $c=0.8$.

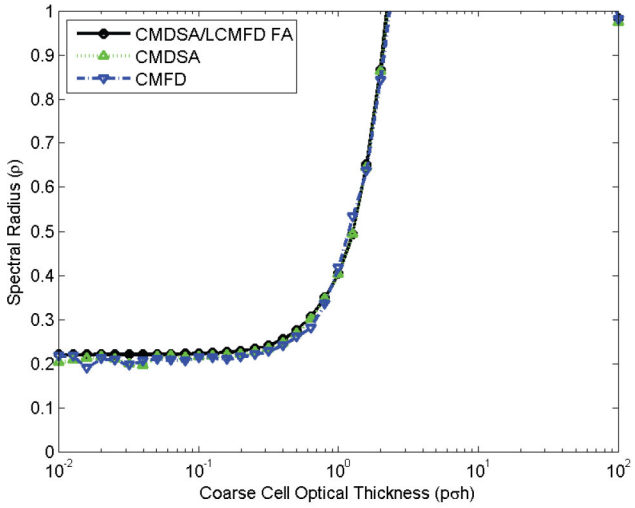

Fig. 12. Spectral radius for $p=3$ and $c=0.99$.

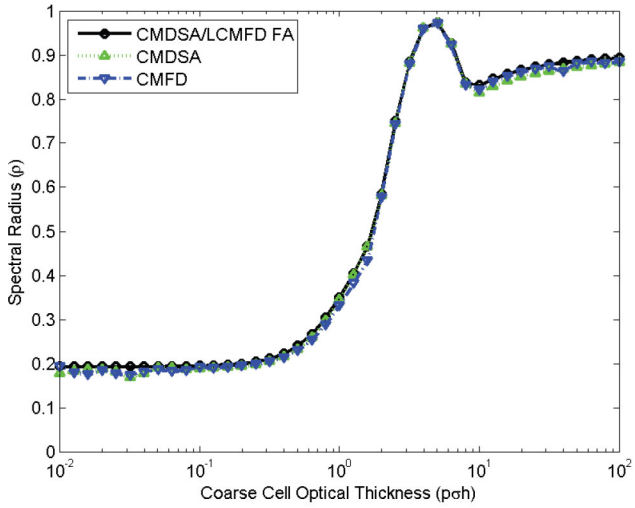

Fig. 11. Spectral radius for $p=3$ and $c=0.9$.

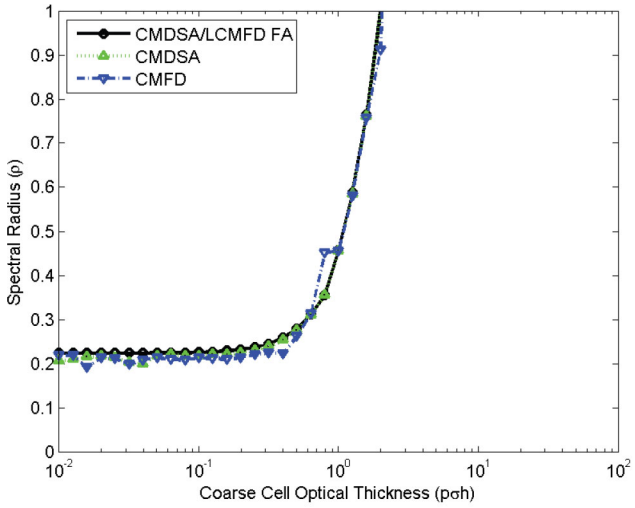

Fig. 13. Spectral radius for $p=3$ and $c=0.9999$.

one-group problems; the practical borderline of instability becomes roughly 2 to 3 mfp (Ref. 15).

2. In the same simulations, CMFD is commonly used with a coarse spatial cell defined to be a *single pin cell*, which is roughly 1 to 2 mfp across and, hence, within multigroup CMFD's practical range of stability. The fine spatial cells (within a coarse cell) are used to resolve the fuel, cladding, and moderator components inside a pin cell. Although CMFD has been successful for reactor physics problems in which a coarse cell is a *single* pin cell, it is not commonly understood that if the coarse grid is enlarged to include *multiple* pin cells, the method can become divergent.

It must be kept in mind that all of the results and discussions in this paper pertain *only* to one-group problems—not to multigroup problems. In this paper we have not even discussed the iteration strategy for multigroup problems (e.g., should the inner iterations be accelerated, and if so, how well or poorly should they be converged?). In practice, a fuel pin (a coarse cell for CMFD) is a small fraction of an mfp across for fast (1 MeV) neutrons but >10 mfp across for low thermal (0.01 eV) neutrons. Therefore, multigroup effects are likely to be significant. If the number of groups used is sufficiently large that the within-group scattering ratios are sufficiently small, our experimental results (Figs. 2, 6, 10, and 14 for $c=0.8$) suggest that the use of CMFD and CMDSA to accelerate the convergence of the within-group equations will be stable. The question then becomes, how will CMFD and CMDSA perform in the

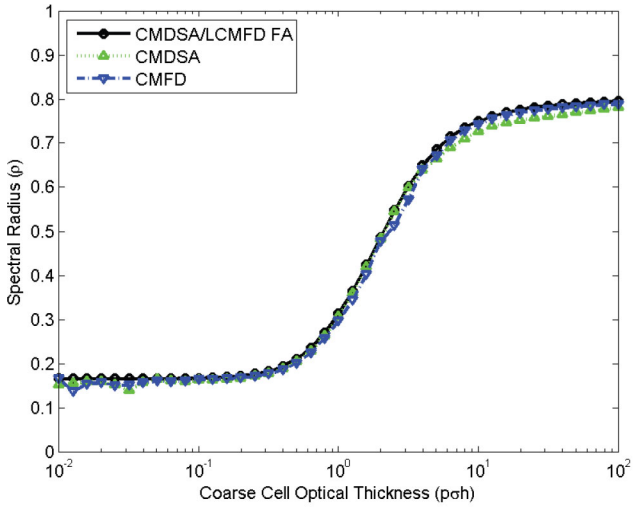

Fig. 14. Spectral radius for $p=4$ and $c=0.8$.

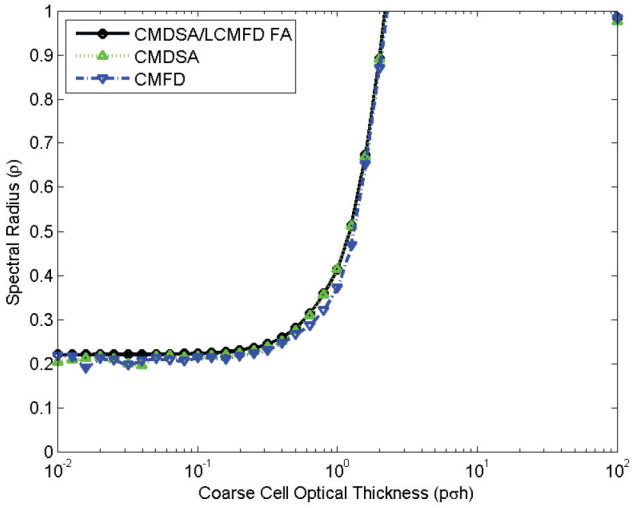

Fig. 16. Spectral radius for $p=4$ and $c=0.99$.

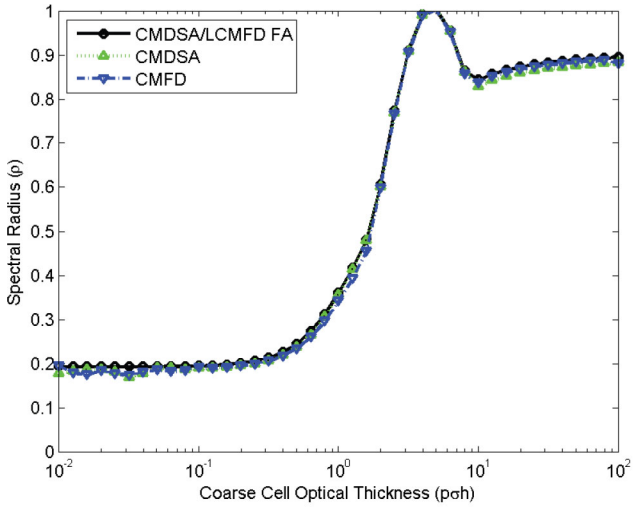

Fig. 15. Spectral radius for $p=4$ and $c=0.9$.

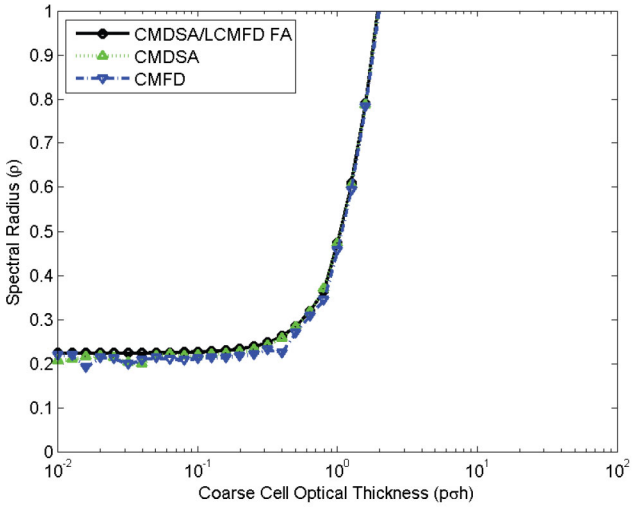

Fig. 17. Spectral radius for $p=4$ and $c=0.9999$.

acceleration of the outer iterations? To our knowledge, this question has never been addressed theoretically. However, CMFD has been observed for certain multigroup problems to be much more stable than for one-group problems. Thus, the theoretical question of multigroup stability for CMFD and CMDSA remains open. The one easy prediction is that whatever the stability properties of CMFD and CMDSA are for multigroup problems, they will be nearly identical.

The results in this paper suggest that for reactor core k-eigenvalue calculations, the CMDSA method could be used to accelerate the convergence of inner iterations (since these are essentially fixed-source problems with a known fission source), while the CMFD method could be used to accelerate the convergence of the outer iterations (since these are not driven by a fixed source). The resulting method would have essentially the same convergence properties as a CMFD code for problems in which CMFD converges. However, because the CMFD/CMDSA method would be insensitive to the occurrence of negative scalar fluxes, which can occur prior to convergence, it would be less likely to diverge for such problems than a code using CMFD for both outer and inner iterations.

Finally, the analysis in this paper suggests that other nonlinear iterative transport methods [such as the pCMFD (partial current-based CMFD) method[16–18]] can also be linearized, to yield corresponding linear iteration methods that have nearly identical convergence properties and that can be Fourier-analyzed. The advantages and

disadvantages of the nonlinear and linearized iterative methods discussed above should also apply to these newer schemes.

In conclusion, the authors wish to express the hope that the contents of this paper will improve the theoretical understanding of the DSA and CMFD methods for reactor physics problems, and that this will lead to practical improvements in the methods.

ACKNOWLEDGMENTS

We gratefully acknowledge support of this research through the U.S. Department of Energy Nuclear Energy University Programs grant DE-AC07-05ID14517.

REFERENCES

1. M. L. ADAMS and E. W. LARSEN, "Fast Iterative Methods for Discrete-Ordinates Particle Transport Calculations," *Prog. Nucl. Energy*, **40**, 3 (2002); http://dx.doi.org/10.1016/S0149-1970(01)00023-3.

2. H. J. KOPP, "Synthetic Method Solution of the Transport Equation," *Nucl. Sci. Eng.*, **17**, 65 (1963); http://dx.doi.org/10.13182/NSE63-1.

3. R. ALCOUFFE, "Diffusion Synthetic Acceleration Methods for the Diamond-Differenced Discrete-Ordinates Equations," *Nucl. Sci. Eng.*, **64**, 344 (1977); http://dx.doi.org/10.13182/NSE77-1.

4. E. W. LARSEN, "Unconditionally Stable Diffusion-Synthetic Acceleration Methods for the Slab Geometry Discrete-Ordinates Equations. Part I: Theory," *Nucl. Sci. Eng.*, **82**, 47 (1982); http://dx.doi.org/10.13182/NSE82-1.

5. D. R. McCOY and E. W. LARSEN, "Unconditionally Stable Diffusion-Synthetic Acceleration Methods for the Slab Geometry Discrete-Ordinates Equations. Part II: Numerical Results," *Nucl. Sci. Eng.*, **82**, 64 (1982); http://dx.doi.org/10.13182/NSE82-2.

6. K. SMITH, "Nodal Method Storage Reduction by Nonlinear Iteration," *Trans. Am. Nucl. Soc.*, **44**, 265 (1983).

7. K. SMITH, "Assembly Homogenization Techniques for Light Water Reactor Analysis," *Prog. Nucl. Energy*, **17**, 303 (1986); http://dx.doi.org/10.1016/0149-1970(86)90035-1.

8. N. Z. CHO and C. J. PARK, "A Comparison of Coarse Mesh Rebalance and Coarse Mesh Finite Difference Accelerations for the Neutron Transport Calculations," *Proc. Conf. Nuclear, Mathematical, and Computational Sciences: A Century in Review, A Century Anew*, Gatlinburg, Tennessee, April 6–11, 2003, American Nuclear Society (2003).

9. Z. ZHONG et al., "Implementation of Two-Level Coarse-Mesh Finite Difference Acceleration in an Arbitrary Geometry, Two-Dimensional Discrete Ordinates Transport Method," *Nucl. Sci. Eng.*, **158**, 289 (2008); http://dx.doi.org/10.13182/NSE06-24TN.

10. E. W. LARSEN and K. W. KELLEY, "CMFD and Coarse-Mesh DSA," *Proc. PHYSOR 2012, Advances in Reactor Physics Linking Research, Industry, and Education*, Knoxville, Tennessee, April 15–20, 2012, American Nuclear Society (2012).

11. G. R. CEFUS and E. W. LARSEN, "Stability Analysis of Coarse-Mesh Rebalance," *Nucl. Sci. Eng.*, **105**, 31 (1990); http://dx.doi.org/10.13182/NSE88-117.

12. G. R. CEFUS and E. W. LARSEN, "Stability Analysis of the Quasidiffusion and Second Moment Methods for Iteratively Solving Discrete-Ordinates Problems," *Transp. Theory Stat. Phys.*, **18**, 493 (1990); http://dx.doi.org/10.1080/00411458908204700.

13. Y. R. PARK and N. Z. CHO, "Coarse-Mesh Angular Dependent Rebalance Acceleration of the Discrete Ordinates Transport Calculations," *Nucl. Sci. Eng.*, **148**, 355 (2004); http://dx.doi.org/10.13182/NSE03-12.

14. Y. R. PARK and N. Z. CHO, "Coarse-Mesh Angular Dependent Rebalance Acceleration of the Method of Characteristics in *x-y* Geometry," *Nucl. Sci. Eng.*, **158**, 154 (2008); http://dx.doi.org/10.13182/NSE06-23.

15. K. SMITH, Personal Communication.

16. N. Z. CHO, G. S. LEE, and C. J. PARK, "Partial Current-Based CMFD Acceleration of the 2D/1D Fusion Method for 3D Whole-Core Transport Calculations, *Trans. Am. Nucl. Soc.*, **88**, 594 (2003).

17. N. Z. CHO, "Fundamentals and Recent Developments of Reactor Physics Methods," *Nucl. Eng. Tech.*, **37**, 25 (2005).

18. K. S. KIM and M. D. DeHART, "Unstructured Partial- and Net-Current Based Coarse-Mesh Finite Difference Acceleration Applied to the Extended Step Characteristics Method in NEWT," *Ann. Nucl. Energy*, **38**, 527 (2011); http://dx.doi.org/10.1016/j.anucene.2010.09.011.